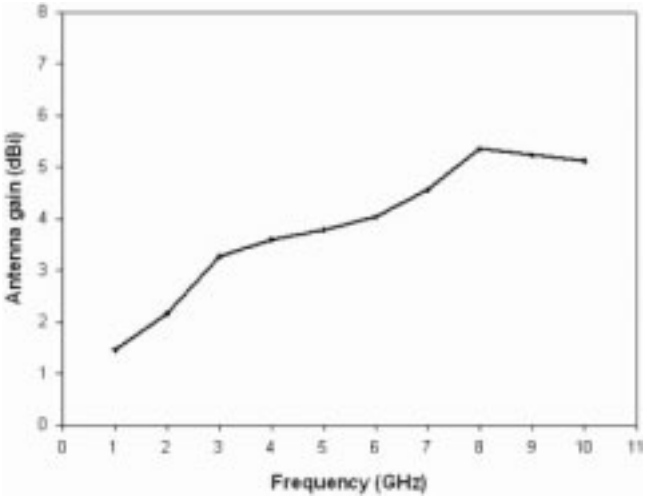


**Figure 7** Measured antenna gain of the proposed antenna


## ACKNOWLEDGMENTS

This work was supported by HY-SDR Research Center at Hanyang University, Seoul, Korea, under the ITRC Program of MIC, Korea.


## REFERENCES


1. F.R. Hsiao and K.L. Wong, An internal ultra-wideband metal-plate monopole antenna for UMTS/WLAN dual-mode mobile phone, Microwave Opt Technol Lett 45 (2004), 265–268.
2. J. Liang, C.C. Chiau, X. Chen, and C.G. Parini, Printed circular disc monopole antenna for ultra-wideband applications, Electron Lett 40 (2004), 1246–1247.
3. K.L. Wong, L.C. Chou, and H.T. Chen, Ultra-wideband metal-plate monopole antenna for laptop application, Microwave Opt Technol Lett 43 (2004), 384–386.
4. M.J. Ammann and Z.N. Chen, Wideband monopole antennas for multi-band wireless systems, IEEE Antennas Propagat Mag 45 (2003), 146–150.
5. W.S. Lee, K.J. Kim, D.J. Kim, and J.W. Yu, Compact frequency-notched wideband planar monopole antenna with a L-shape ground plane, Microwave Opt Technol Lett 46 (2005), 563–566.
6. S.W. Su, K.L. Wong, Y.T. Cheng, and W.S. Chen, Finite-ground-plane effects on the ultra-wideband planar monopole antenna, Microwave Opt Technol Lett 43 (2004), 535–537.
7. S.H. Choi, J.K. Park, S.K. Kim, and J.Y. Park, A new ultra-wideband antenna for UWB applications, Microwave Opt Technol Lett 40 (2004), 399–401.
8. K.H. Chung, T.Y. Yun, and J.H. Choi, Wideband CPW-fed monopole antenna with parasitic elements and slots, Electron Lett 40 (2004), 1038–1040.
9. Ansoft High-Frequency Structure Simulation (HFSS) ver 9.2, Ansoft Corporation.


© 2006 Wiley Periodicals, Inc.

# ACCURATE MODELING OF THE CYLINDRICAL WIRE KERNEL


**Anuraag Mohan and Daniel S. Weile**
Department of Electrical and Computer Engineering
140 Evans Hall
University of Delaware
Newark, DE 19716


*Received 11 October 2005*


**ABSTRACT:** *Many existing numerical techniques used to analyze wire antennas assume the current distribution on the wire to be one-dimensional (1D). This assumption imposes geometric constraints on the ratio of the wire radius to the discretized antenna segment length. Moreover, many kernel approximations are so inaccurate that higher-order basis functions for wire modeling are unthinkable. More accurate kernel models are possible, but generally result in infinite series or require complicated integration rules. This work presents a new generalized approach to the modelling of cylindrical wire antennas. The method is not plagued by the aforementioned geometric restrictions and can be extended to model the higher-order behavior of wires. The numerical results show the method to be both stable and robust.* © 2006 Wiley Periodicals, Inc. Microwave Opt Technol Lett 48: 740–744, 2006; Published online in Wiley InterScience (www.interscience.wiley.com). DOI 10.1002/mop.21461


**Key words:** *cylindrical wire kernel; wire antennas; method of moments*

## 1. INTRODUCTION

Wire scatterers are among the most studied topics in computational electromagnetics, since the unknown is essentially one dimensional (1D): by definition, a wire is much larger in one dimension than in the other two [1–13]. Classic techniques for analyzing these structures rely on the method of moments (MoM) to solve the electric-field integral equation (EFIE) [14]. Wire techniques are distinguished from other MoM-based analyses in that they assume that the current may be modeled as flowing in only one direction—along the wire.

The oldest wire-scattering analysis technique assumes a filamentary current. Because the field radiated by a filament cannot be integrated, the basis and testing functions are displaced by the radius of the wire. This "thin-wire approximation" imposes a strict restriction on the length-to-radius ratio of the discretized antenna segment. Moreover, since the reduced kernel approximation is inherently low-order, it precludes the use of higher-order basis functions. This difficulty can be profound, especially when the wires are included in a more complex model incorporating high-order discretized surfaces. Nonetheless, these techniques have been used to accurately model wire-based and wire-meshed structures [15, 16].

Subsequent research has proposed an infinite-series expansion approach to model a cylindrical wire kernel with constant and linear current distribution [17–19]. Since this work models a cylindrical wire kernel, it is not as constrained by the thin-wire condition. (Of course, in failing to account for either azimuthal currents or variations, it must still be somewhat limited. This limitation, however, is in keeping with the distinction between wires and general surfaces.) Similarly, a variant of the Duffy transform can be used to extract the singularity from the 2D cylindrical kernel [20]. Both of these approaches are a vast improvement over the thin wire technique, but both seem to overcomplicate what appears at first glance to be a simple 1D problem.

This work proposes a new accurate and simple approach for the modeling of cylindrical wire antennas. Section 2 introduces a technique for evaluating the fields due to a constant current cylindrical antenna. This technique will then be extended to model linear distribution current using the Method of Moments (MoM). In section 3, the accuracy and validity of the proposed technique are proven by comparison with the reduced-kernel approach and experimental results.

## 2. FORMULATION

This section discusses the formulation of the problem at hand. Subsection 2.1. presents the new method for integrating the singular wire kernel. The method of moments (MoM) implementation of this approach is covered in subsection 2.2.

### *2.1. Wire Antennas*

The cylindrical wire segment under consideration is illustrated in Figure 1. The wire is aligned along the $z$-axis. The radius of the wire is $a$ and the length of the segment is $\Delta$. The surface current density $J_z$ is assumed to be azimuthally invariant. The magnetic vector potential for this antenna is given by [19]:

$$A_z(\rho, z) = \frac{\mu}{4\pi}\int_{-\Delta/2}^{\Delta/2} I(z')\,K(\rho, z-z')dz'. \tag{1}$$

The cylindrical wire kernel $K(\rho, z - z')$ is expressed as

$$K(\rho, z-z') = \frac{1}{2\pi}\int_{-\pi}^{\pi} \frac{e^{-j\beta R'(\rho,\phi,z-z')}}{R'(\rho, \phi, z-z')}\,d\phi. \tag{2}$$

The term $R'(\rho, \phi, z - z')$ is the distance between the source point $(a, \phi', z')$ and the field point $(\rho, \phi'', z)$, and is given by

$$R'(\rho, \phi, z-z') = \sqrt{(z-z')^2 + \rho^2 + a^2 - 2\rho a\cos\phi}, \tag{3}$$

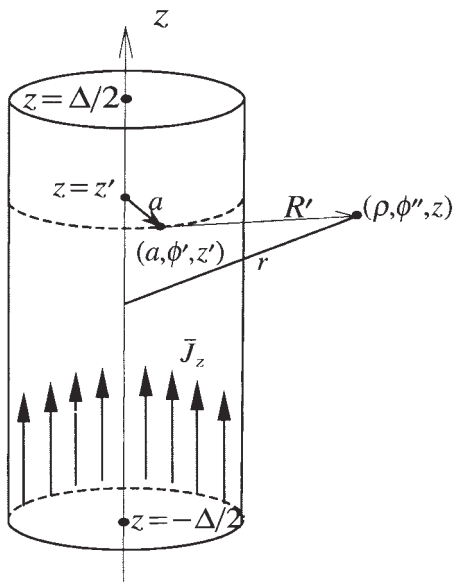


**Figure 1** Geometry of a cylindrical antenna segment

where the source point is $(a, \phi', z')$, the field point is $(\rho, \phi'', z)$, and $\phi = \phi' - \phi''$. In the subsequent discussion, where the dependence of a function is clear from the context, it will be omitted.

For a constant current distribution $I(z') = I_0$, Eq. (1) becomes simply

$$A_z^0(\rho, z) = \frac{\mu I_0}{4\pi}\int_{-(\Delta/2)}^{\Delta/2}\int_{-\pi}^{\pi} \frac{e^{-j\beta R'}}{2\pi R'}\,d\phi dz'. \tag{4}$$

If the observation point is not on the wire, the integral is not singular and can be easily integrated by a host of methods. On the other hand, special care is required when $\rho = a$, so this case will be assumed for the remainder of this section. When $\rho = a$, the integrand in Eq. (4) has a singularity that can be extracted by rewriting the equation as follows:

$$A_z^0(a, z) = \frac{\mu I_0}{4\pi}\left\{\underbrace{\frac{1}{2\pi}\int_{-(\Delta/2)}^{\Delta/2}\int_{-\pi}^{\pi}\frac{1}{R'(a, \phi, z-z')}\,d\phi dz'}_{I_1^0(z)}\right.$$
$$\left. + \underbrace{\frac{1}{2\pi}\int_{-(\Delta/2)}^{\Delta/2}\int_{-\pi}^{\pi}\frac{e^{-j\beta R'(a,\phi,z-z')}-1}{R'(a, \phi, z-z')}\,d\phi dz'}_{I_2^0(z).}\right\}. \tag{5}$$

The first term in the above expression is singular when the source and field points are the same. The term $I_2^0(z)$ is always well-behaved and can be evaluated numerically without any special treatment.

The singular term $I_1^0(z)$ can be rewritten by interchanging the order of integration, applying the change of variables, and changing the azimuthal variable to $\theta = \phi/2$. After noting the symmetry present in the $\theta$ integration, $I_1^0(z)$ becomes

$$I_1^0(z) = \frac{2}{\pi}\int_0^{\pi/2}\int_{-(\Delta/2)}^{\Delta/2}\frac{d\theta dz'}{R'(z-z',\,\theta)}, \tag{6}$$

where

$$R'(z-z',\,\theta) = \sqrt{(z-z')^2 + 4a^2\sin^2\theta}. \tag{7}$$

Applying the change in variables $\xi = z' - z$, separating out the potential singularity at $z = z'$, and using symmetry about $\xi = 0$ results in the expression

$$I_1^0(\rho, z) = \frac{4}{\pi}\int_0^{\pi/2}\int_0^{\xi_1}\frac{1}{R'(\xi,\,\theta)}\,d\xi d\theta$$
$$\underbrace{\qquad\qquad}_{Singular\ at\ \xi=0,\theta=0}$$
$$-\frac{2}{\pi}\int_0^{\pi/2}\int_{\xi_1-2z}^{\xi_1}\frac{1}{R'(\xi,\,\theta)}\,d\xi d\theta, \tag{8}$$

where $2\xi_1 = \Delta + 2z$. The nonsingular (second) integral in the above expression can be evaluated using a numerical-quadrature

technique. The $\xi$-integration of Eq. (8) can be performed analytically, yielding [21, 22]:

$$\frac{4}{\pi}\int_0^{\pi/2}\int_0^{\xi_1}\frac{1}{R'(\xi,\,\theta)}\,d\xi d\theta=\frac{4}{\pi}\int_0^{\pi/2}\ln(\xi_1+R'(\xi_1,\,\theta))d\theta + 2\ln\left[\frac{\xi_1}{a}\right]. \quad (9)$$

All of the terms in this expression are nonsingular, and the integral can be evaluated numerically.

The analysis of a wire with linear current distribution $I(z')=J_0z'$ is analogous to the scheme used for constant current distribution. The vector potential for this case is given by the following expression:

$$A_z^1(\rho,\,z)=\frac{\mu J_0}{4\pi}\left\{\underbrace{\frac{1}{2\pi}\int_{-(\Delta/2)}^{\Delta/2}\int_{-\pi}^{\pi}\frac{z'}{R'(a,\,\phi,\,z-z')}\,d\phi dz'}_{I_1^1(z)} + \underbrace{\frac{1}{2\pi}\int_{-(\Delta/2)}^{\Delta/2}\int_{-\pi}^{\pi}\frac{z'(e^{-j\beta R'(a,\phi,z-z')}-1)}{R'(a,\,\phi,\,z-z')}\,d\phi dz'}_{I_2^1(z).}\right\}. \quad (10)$$

The nonsingular term $I_1^2(\rho,\,z)$ can be evaluated numerically, while the singular term $I_1^1(\rho,\,z)$ is rewritten (using transformations similar to the above) as

$$I_1^1(z)=\frac{2}{\pi}\int_0^{\pi/2}\int_{-\xi_1}^{-\xi_1+\Delta}\frac{\xi}{R'(\xi,\,\theta)}\,d\xi d\theta+zI_1^0(z), \quad (11)$$

where $R'(\xi,\,\theta)$ and $\xi_1$ retain their values from Eq. (8). Evaluating the inner integral in this equation analytically gives [21]:

$$I_1^1(z)=\frac{2}{\pi}\int_0^{\pi/2}[\sqrt{(-\xi_1+\Delta)^2+4a^2\sin^2\theta}-\sqrt{\xi_1^2+4a^2\sin^2\theta}]d\theta + zI_1^0(z). \quad (12)$$

The new integral in this term can be evaluated using any standard numerical-quadrature rule for nonsingular integrands. Thus, the methods covered here reduce all of the integrals encountered in a MoM implementation to integrals that can be easily and accurately performed by Gaussian (specifically, Gauss–Legendre) integration.

### *2.2. Method of Moments*

The results of the previous section can easily be used in a MoM code for modeling wires. Assuming that the wire is straight and $z$-directed, the EFIE for scattering from the wire is given by [23]:

$$E^{inc}(z)=j\omega\mu\int_{z'}I(z')\,K(z-z')dz'-\frac{1}{j\omega\varepsilon}\frac{d}{dz}\int_{z'}\frac{dI(z')}{dz'}\,K(z-z')dz', \quad (13)$$

where $\omega$, $\mu$, and $\varepsilon$ represent angular frequency, permeability, and permittivity, respectively. To apply the MoM, the current on a wire is approximated by a linear combination of basis functions:

$$I(z')\approx\sum_{n=1}^{N}I_nB_n(z'), \quad (14)$$

where $B_n(z')$ is the basis function and $I_n$ is the unknown basis function weighting coefficient associated with it. The basis functions used here are given by

$$B_n(z')=\begin{cases}B_n^+(z')=\dfrac{z'}{\Delta_n^+}, & z'\text{ in }S_n^+\\ B_n^-(z')=1-\dfrac{z'}{\Delta_n^-}, & z'\text{ in }S_n^-\\ 0, & \text{otherwise}\end{cases}, \quad (15)$$

where $\Delta_n^{\pm}$ is the length of segment $S_n^{\pm}$ and the superscript denotes the slope of basis functions. This arrangement is illustrated in Figure 2. Eqs. (14) and (15) are then substituted into Eq. (13), which is subsequently multiplied by each basis function in turn and integrated over the wire. This process yields a matrix equation $\mathbf{ZI}=\mathbf{E}$ in which the vector $\mathbf{I}$ contains the basis-function coefficients and vector $\mathbf{E}$ contains the incident-field information. (Specifically, the elements of $\mathbf{E}$ are just the incident field multiplied by the basis function and integrated over the surface of the wire.) The values of the elements of the $\mathbf{Z}$ matrix are computed by the following expression:

$$z_{mn}=j\omega\mu\int_{z_1}^{z_2}B_m(z)\cdot\int_{z'}B_n(z')\,K(z-z')dz'dz + \frac{1}{j\omega\varepsilon}\int_{z_1}^{z_2}\frac{dB_m(z)}{dz}\cdot\int_{z'}\frac{dB_n(z')}{dz'}\,K(z-z')dz'dz - \frac{1}{j\omega\varepsilon}B_m(z)\cdot\int_{z'}\frac{dB_n(z')}{dz'}\,K(z-z')dz'\Big|_{z_1}^{z_2}. \quad (16)$$

The diagonal elements of the matrix (corresponding to the self-term) can be evaluated using the scheme presented in subsection 2.1., since the basis-function integrations only involve linear or constant functions. The kernel integrals for off-diagonal elements can be expressed as elliptic integrals, and evaluated using standard numerical techniques [19, 24].

## 3. NUMERICAL RESULTS

This section demonstrates the accuracy of results obtained by the proposed technique, and compares the kernel-integration method considered here to the reduced-kernel method. In particular, the results presented here focus on the convergence of different

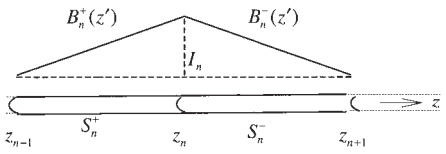


**Figure 2** Basis functions associated with a wire segment

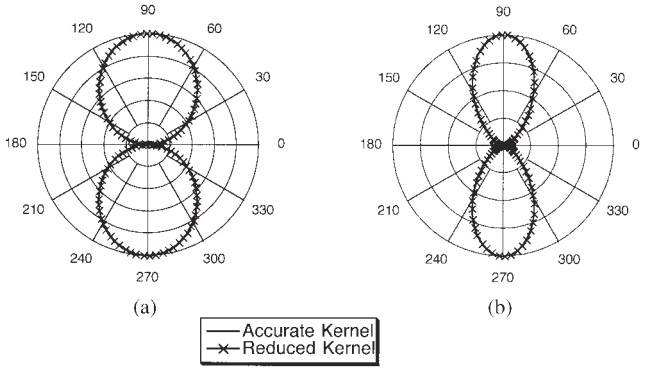


**Figure 3** Comparison of far-field pattern obtained by the two techniques for (a) a half-wave dipole and (b) a full-wave dipole

schemes as the wire is further discretized. All the simulations will assume delta-gap excitation at the center of the antenna.

Figures 3(a) and 3(b) compare the normalized far-field pattern returned by the proposed technique and the thin-wire approach for a half-wave dipole and a full-wave dipole, respectively. The antenna length to radius ratio $L/a$ for these dipoles is 150. Thirty segments are used to model current flow on the antenna, making the segment-to-radius ratio $\Delta/a \approx 5$. One can see an excellent correspondence in the results obtained by the two techniques.

Figure 4 compares the antenna current returned by the two techniques for a highly discretized full-wave dipole. The antenna has been discretized into 150 segments with a segment-to-radius ratio $\Delta/a = 1$. The graph illustrates the breakdown of the reduced-kernel technique for this level of discretization. On the other hand, the current obtained by the proposed technique for high discretization compares well with results for coarser discretization.

Finally, Figure 5 compares the input conductance calculated by the proposed technique with available experimental data [5, 25]. The numerical results match the experimental data for a wide range of wavelengths. The ratio of the wire radius to the wavelength $a/\lambda$ is kept constant at $7.002 \times 10^{-3}$. The wire is discretized into 50 segments and the segment length-to-radius ratio $\Delta/a$ for this test varies from 0.9 to 2.85 as the frequency of operation changes. This result reflects the accuracy of the numerical technique, even at high levels of discretization.

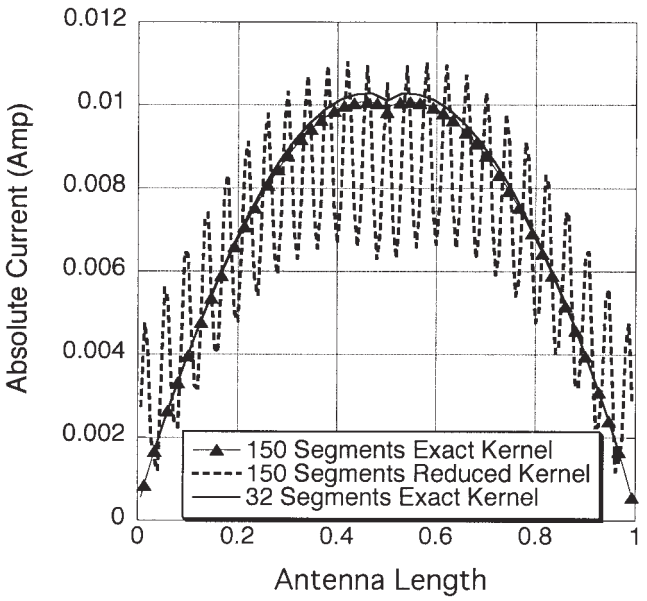


**Figure 4** Comparison of current distribution along the antenna length for varying discretization

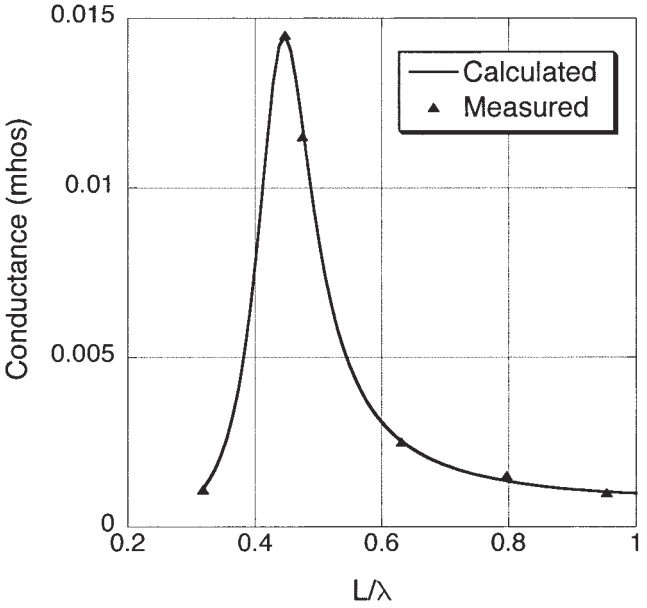


**Figure 5** Experimental vs. calculated input conductance for cylindrical antennas

## 4. CONCLUSION

This study has proposed a new integration method for a wire kernel, assuming constant or linear basis functions. This scheme is not limited to coarse discretizations such as the classical reduced-kernel approach. Moreover, the integration scheme is exact and the only approximations it makes pertain to the quadrature scheme used to evaluate the integrals. The numerical results presented confirm these claims.

The technique presented here can be extended to model composite wire structures using higher-order basis functions and also to model transient wire scattering [26]. These applications will be discussed by the authors in a future contribution.

## REFERENCES

1. C.M. Butler and D.R. Wilton, Analysis of various numerical techniques applied to thin-wire scatterers, IEEE Trans Antennas Propagat AP-23 (1975), 534–540.
2. D.C. Chang, On the electrically think antennas, Radio Sci 2 (1967), 1043–1060.
3. R.H. Duncan and F.A. Hinchey, Cylindrical antenna theory, J Res Natl Bur Standards 64D (1960), 569–584.
4. R.W.P. King, The theory of linear antennas, Harvard University Press, Cambridge, MA, 1956.
5. R.W.P. King, The linear antenna: Eighty years of progress, Proc IEEE 55 (1967), 2–26.
6. R.W.P. King and T.T. Wu, The thick tubular transmitting antenna, Radio Sci 2 (1967), 1061–1065.
7. K.K. Mei, On the integral equations of thin wire antennas, IEEE Trans Antennas Propagat AP-13 (1965), 374–378.
8. E.K. Miller and F.J. Deadrick, Some computational aspects of thin-wire modeling, Numerical and asymptotic techniques for electromagnetics, R. Mittra (Ed.), Springer-Verlag, New York, 1975.
9. A.F. Peterson, Difficulties encountered when attempting to validate thin-wire formulations for linear dipole antennas, J Appl Computat Electromagn Soc (ACES) 4 (1989), 25–40.

10. B.D. Popovic, M.B. Dragovic, and A.R. Djordjevic, Analysis and synthesis of wire antennas, Wiley, New York, 1982.
11. J.H. Richmond, Radiation and scattering by thin-wire structures in the complex frequency domain, E.K. Miller, L. Medgyesi-Mitschang, and E.H. Newman (Eds.), Computational electromagnetics, IEEE Press, New York, 1992.
12. P.G. Rogers and M.W. Gunn, An entire-domain Galerkin analysis of the moderately thick dipole, IEEE Trans Antennas Propagat AP-28 (1980), 117–121.
13. G.A. Thiele, Wire antennas, R. Mittra (Ed.), Computer techniques for electromagnetics, Pergamon, New York, 1973.
14. R.F. Harrington, Field computation by moments methods, Macmillan, New York, 1968.
15. G.J. Burke and A.J. Poggio, Numerical electromagnetics code (NEC): Method of moments, Technical Document 116, Naval Ocean System Center, San Diego, CA, 1981.
16. A.C. Ludwig, Wire grid modeling of surfaces, IEEE Trans Antennas Propagat AP-35 (1987), 1045–1048.
17. D.H. Werner, An exact formulation for the vector potential of a cylindrical antenna with uniformly distributed current and arbitrary radius, IEEE Trans Antennas Propagat 41 (1993), 1009–1018.
18. D.H. Werner, A method of moments approach for the efficient and accurate modeling of moderately thick cylindrical wire antennas, IEEE Trans Antennas Propagat 46 (1998), 373–382.
19. D.H. Werner, J.A. Huffman, and P.L. Werner, Techniques for evaluating the uniform current vector potential at the isolated singularity of the cylindrical wire kernel, IEEE Trans Antennas Propagat 42 (1994), 1549–1553.
20. D.R. Wilton and M.A. Khayat, Evaluation of singular and near-singular potential integrals, IEEE AP-S Int Symp and URSI Radio Sci Mtg, Columbus, OH, 2003.
21. I.S. Gradshteyn and I.M. Ryzhik, Table of integrals, series, and products, A. Jeffrey (Ed.), 5th ed., Academic Press, London, 1994, pp. 104–105.
22. I.S. Gradshteyn and I.M. Ryzhik, Table of integrals, series, and products, A. Jeffrey (Ed.), 5th ed., Academic Press, London, 1994, pp. 614–615.
23. A.F. Peterson, S.L. Ray, and R. Mittra, Computational methods for electromagnetics, Wiley–IEEE Press, New York, 1997.
24. M. Abramowitz and I.A. Stegun, Handbook of mathematical functions with formulas, graphs, and mathematical tables, Dover Publications, New York, 1972.
25. R.B. Mack, A study of circular arrays, Ph.D. thesis, Harvard University, Cambridge, MA, 1963.
26. G. Pisharody and D.S. Weile, Electromagnetic scattering from a homogeneous material body using time-domain integral equation and bandlimited extrapolation, IEEE Antennas Propagat Soc AP-S Int Symp Dig 3 (2003), 567–570.

© 2006 Wiley Periodicals, Inc.

# MODIFIED PULSE SHAPER DESIGN WITH PICOSECOND DURATION AND WIDEBAND RESPONSE FOR UWB APPLICATIONS

**Ji-Chyun Liu,[1] Shuh-Tai Lu,[1] Ching-Yang Wu,[2] Chin-Yen Liu,[2] and Ming-Hsun Chiang[2]**
[1] Dept. of Electrical Engineering
Ching Yun University
Jung-Li, Taoyuan, Taiwan
[2] Dept. of Electrical Engineering
Chung Cheng Institute of Technology
National Defense University
Tashi, Taoyuan, Taiwan

*Received 7 October 2005*

**ABSTRACT:** *A simple, compact pulse shaper of inverse Gaussian monocycle with picosecond duration and wideband response is proposed in this paper. By modifying the conventional pulse shaping circuit, the pulse shaper utilizes the RC differentiator and Schottky diode to construct the clamping circuit, and form an inverse Gaussian monocycle pulse. In addition, the short-stub is used for constructing the resistive matching network as well as adjusting the shape of inverse Gaussian monocycle pulse. In applications, an ultra-short inverse Gaussian monocycle pulse with duration of 600 ps, symmetry of 100%, and ring level of 5.8% has been obtained. Meanwhile, the frequency response presents the characteristic of wideband spectrum with a −3-dB BW of 141.7%. Both the measured and simulated results are in good agreement with the time and frequency responses.* © 2006 Wiley Periodicals, Inc.
Microwave Opt Technol Lett 48: 744–749, 2006; Published online in Wiley InterScience (www.interscience.wiley.com). DOI 10.1002/mop.21462

**Key words:** *pulse shaper; inverse Gaussian monocycle pulse; short-stub*

## 1. INTRODUCTION

Recently, ultra-wideband (UWB) communications have been developed as a good and cost-effective method for short range, especially in building systems [1, 2]. Basically, it is a carrier-free communication in which baseband messages are contained in the narrow pulse. Restated, only the shaped pulse is transmitted and received between the terminals, and it is called the "impulse radio" for applications [3–6]. The pulse duration is usually in the range of a picosecond. Thus, the ultra-short pulse-shaping circuit is a main research topic in UWB systems [7–12].

Generally, step, Gaussian, and Gaussian monocycle pulses are applied in UWB systems due to the common characteristic of UWB spectrum. Several possible monocycle pulses, including Gaussian monocycle, Scholtz's monocycle, Manchester monocycle, Sine monocycle, rectangular monocycle, and so forth, have been developed. However, the spectrum of the Gaussian monocycle pulse does not includes the dc portion and low-frequency parts for applications [2]. Basically, Gaussian monocycle pulse-shaping circuits consist of a step-recovery diode (SRD), an RC differentiator, and a time-delay line. Therefore, the attractive features of these pulse-shaping circuits are simplicity, compact size, and low cost.

In this paper, based on the modified conventional monocycle pulse-shaping circuit, we propose a novel inverse Gaussian monocycle pulse shaper with picosecond pulse duration and wideband spectrum. Based on the RC differentiator and Schottky diode, the clamping circuit is constructed, and the inverse Gaussian monocycle pulse is formed. Meanwhile, we employ the short-stub for establishing the resistive matching network as well as adjusting the